Annals of Nuclear Energy 120 (2018) 304–318

Contents lists available at ScienceDirect

Annals of Nuclear Energy

journal homepage: www.elsevier.com/locate/anucene

Fuel performance of chromium-coated zirconium alloy and silicon carbide accident tolerant fuel claddings

Malik Wagih [a], Benjamin Spencer [b], Jason Hales [b], Koroush Shirvan [a,*]

[a] Department of Nuclear Science and Engineering, Massachusetts Institute of Technology, 77 Massachusetts Ave, Cambridge, MA 02139, USA
[b] Fuel Modeling and Simulation, Idaho National Laboratory, P.O. Box 1625, Idaho Falls, ID 83415-3840, United States

ARTICLE INFO

Article history:
Received 27 March 2018
Received in revised form 31 May 2018
Accepted 1 June 2018
Available online 14 June 2018

Keywords:
Accident tolerant fuel
Chromium
Silicon carbide
Cladding
Nuclear fuel
BISON

ABSTRACT

The U.S. Department of Energy's Accident Tolerant Fuel program is focused on extending the time for fuel failure during postulated severe accidents compared to the standard UO_2-Zr alloy fuel system. This paper investigates the feasibility of two different chromium-coated cladding concepts, one of which is zirconium-alloy based and the other is composite-SiC based. Both claddings had 50 μm coatings, deducted from the base layer thicknesses. The claddings were studied, using the multi-physics fuel performance tool BISON, under steady-state PWR operating conditions as well as under two transients: a power ramp and a loss-of-coolant accident (LOCA). The chromium-coated claddings showed comparable thermo-mechanical performance to the reference Zircaloy-4 cladding. As chromium is reported to provide an order of magnitude improvement in oxidation resistance, it is expected to be a better alternative in accident scenarios. Simulation results for both concepts show that further experimental investigation as well as modeling of beyond design-basis accidents is warranted.

1. Introduction

The Fukushima accident in 2011, triggered by a massive 9.0 magnitude earthquake followed by a tsunami, had a devastating effect on the status and prospects of nuclear power worldwide. Alarmed by the incident and the following large release of radioactive material to the atmosphere and the surrounding land and ocean (Stohl et al., 2012), Japanese authorities mandated a shutdown of its nuclear capacity (Huenteler et al., 2012). Longer term effects included Japan's later announcement of plans to reduce dependency on nuclear power and to revise their Basic Energy Plan (Huenteler et al., 2012). In addition, Germany and Switzerland have announced plans to phase-out nuclear energy in the foreseeable future (Jorant, 2011).

As a result of the accident, a renewed interest was generated in addressing the shortcomings of the traditional zirconium-based (so-called "Zircaloy") claddings under accident conditions. Current light water reactors (LWRs) use a fuel system composed of uranium dioxide (UO_2) pellets, zirconium-alloy cladding and a helium filled pellet-cladding gap. The choice of zirconium alloys as the primary cladding material is due to its low neutron absorption, good corrosion resistance and structural integrity under operating conditions (Lemaignan, 2012). However, under design-basis accidents (DBAs) and beyond DBAs, zirconium alloys can rapidly lose their integrity due to their interaction/oxidation in high-temperature steam (Terrani et al., 2014). This has led to a large research effort to mitigate and possibly eliminate high temperature oxidation of the fuel system currently used in LWRs. The proposed solutions are called accident tolerant fuels (ATFs) (Zinkle et al., 2014).

ATFs are fuels which in comparison with the standard UO_2-Zr system, can tolerate loss of active cooling in the core for a considerably longer time period (depending on the LWR system and accident scenario) while maintaining or improving the fuel performance during normal operations (Carmack et al., 2013). These improved properties are mainly focused on reducing the oxidation rate and hydrogen (or other combustible gases) production at high temperatures. Additional, targeted improvements include increasing the cladding melting point and its strength at high temperature in comparison to current Zircaloy cladding. Improvements to the fuel are also under investigation, especially in the areas of improved fission gas retention, higher temperature margin to fuel melt and increased thermal conductivity (Zinkle et al., 2014).

Numerous candidates are currently under investigation as alternatives to the UO_2-Zr system. To list a few, Pint et al. (2015) looked into the oxidation kinetics of FeCrAl, SiC, Molybdenum and MAX-phase alloys (Ti_3SiC_2, Ti_2AlC). Deck et al. (2015) experimentally

* Corresponding author.
E-mail address: kshirvan@mit.edu (K. Shirvan).

https://doi.org/10.1016/j.anucene.2018.06.001
0306-4549/

investigated SiC properties for ATF deployment. Mo-Zr and Mo-FeCrAl duplex claddings were investigated by Cheng et al. (2016). Iron based alloys have been proposed by Terrani et al. (2014). Extensive experimental investigation of FeCrAl properties is being carried out mainly by Oak Ridge National Laboratory (Yamamoto et al., 2015; Field et al., 2015; Field et al., 2017). Recently, Gamble et al. (2017) investigated FeCrAl claddings under PWR normal operating and loss-of-coolant conditions, as have Wu et al. (2015) and Galloway et al. (Galloway and Unal, 2016). Chromium-coated claddings have been studied by Ševeček et al. (2018), Shah et al. (2017), Koo et al. (2014), Brachet et al. (2017, 2015, 2014) and Katoh et al. (2017). This list is not complete by any means but rather highlights the magnitude of the current research efforts (both experimental and modeling and simulation) and identifies some of the promising candidates.

The focus of this paper is to investigate two proposed Chromium-coated ATF cladding system concepts, using thermo-mechanical modeling under both steady-state and transient conditions. The aim of this investigation is to compare the performance of each concept relative to a standard Zirconium alloy cladding. The most promising concepts could be then further investigated experimentally to test their performance and possible performance enhancement under simulated accident conditions. Further experimentation would also provide more data for feedback into the modeling/simulation codes, as data is one of the limitations to developing physical/realistic models. However, as experiments are rather costly and time intensive, it is essential to limit them to the most promising ATF concepts and to determine the properties that have the greatest impact on performance. Therefore, simulations and modeling can help focus the experimental efforts and provide an informed judgement on the concepts expected to be the most promising.

2. Methodology

The multi-physics fuel performance tool BISON (Williamson et al., 2012) is used for the thermo-mechanical modeling of the fuel concepts considered in this paper. BISON is a finite element-based nuclear fuel performance code built on the MOOSE framework (Gaston et al., 2009), which is a framework capable of solving general systems of coupled non-linear equations. The BISON code is capable of solving the fully coupled thermo-mechanics and diffusion equations for multidimensional (up to 3D) representations of the geometry. The code includes fuel models that represent temperature and burnup dependent material properties, such as swelling, fuel densification, thermal and mechanical properties, fission gas production and release, and irradiation and thermal creep. Models for several cladding materials are included as well, such as Zricaloy-2/4. The standard set of models for material behavior are augmented by this work, which added models for additional materials including Chromium and Silicon Carbide. These material properties were coded using object oriented C++ and added as new modules in the program, and are described in Section 3.

2.1. ATF concepts

The paper will focus on two types of cladding, Zirc-4 based cladding and SiC based cladding, as shown in Fig. 1. The coating thickness is limited to 50 μm in both cases. The SiC cladding dimensions shown in Fig. 1 were kept constant for all cases in this study. For the Zr4 cladding, the Zircaloy thicknesses varied slightly for each simulation as we attempted to re-create experimental conditions. The thickness of the coating for Zr4 cladding is stated in the test description for each simulation. The simulations will compare the performance of each ATF concept against a reference Zr4 cladding. The fuel-systems will be subjected to steady state simulations, followed by power ramps, and finally LOCA simulations.

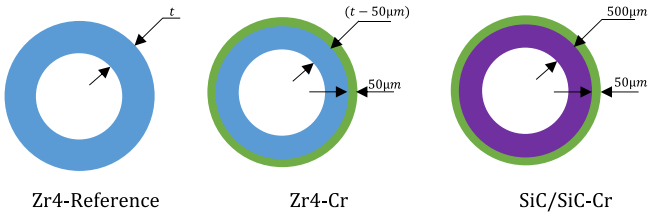

Fig. 1. Different Zr4-based claddings and proposed coating thicknesses.

3. Material properties

3.1. Chromium

Pure chromium properties are not commonly studied, as it is usually used as an alloying element. This section compiles properties for chromium and discusses the limitations of the data. For this section, temperature (T) is in units of Kelvin unless stated otherwise.

3.1.1. Thermal properties

Thermal properties were obtained for commercially available pure chromium Ducropure (trademark of Metallwerke Plansee AG, Austria) (Holzwarth and Stamm, 2002). The Specific heat (C_p) in the range between 300 and 1300 K is expressed as (Holzwarth and Stamm, 2002):

$$C_P(T) = (-1.28 \times 10^{-7}T^3 + 3.39 \times 10^{-4}T^2 - 0.09T + 483.2)J.kg^{-1}K^{-1} \quad (1)$$

Thermal Conductivity (between 300 and 1300 K) (Holzwarth and Stamm, 2002):

$$\lambda(T) = (-2.07 \times 10^{-8}T^3 + 4.85 \times 10^{-5}T^2 - 0.06T + 101.75)WK^{-1}m^{-1} \quad (2)$$

3.1.2. Mechanical properties

The Elastic Modulus as a function of temperature E(T) (between 300 and 1500 K) is extracted from (Armstrong Harry, 1964). The data can be fitted to the following polynomial:

$$E(T) = (-2.50 \times 10^{-5}T^2 - 0.01T + 264.11)GPa \quad (3)$$

with R^2 = 0.9934. At room temperature, Eq. (3) gives a value of ~261 GPa which is in close proximity to values obtained from nanoindentation of Cr coating (233.6 ± 26.4 GPa) that was exposed to steam oxidation at 500 °C for 20 days (Ševeček et al., 2018).

The Poisson's ratio can be approximately considered as a constant (Simmons, 1965):

$$v = 0.22 \quad (4)$$

The mean thermal expansion coefficient (between 300 and 1300 K), with a reference temperature of 293 K is (Holzwarth and Stamm, 2002):

$$\alpha(T) = (1.27 \times 10^{-10}T^3 + 5.41 \times 10^{-7}T^2 + 0.0015T + 7.87) \times 10^{-6}K^{-1} \quad (5)$$

3.1.3. Thermal creep

The thermal creep rate of chromium can be calculated using a Norton creep law:

$$\dot{\epsilon} = A \exp\left(-\frac{Q}{RT}\right).\sigma^n \quad (6)$$

where $\dot{\epsilon}$ is the creep rate (s^{-1}), σ the effective stress (Pa) and T (K) is the temperature, A is the pre-exponential coefficient of creep, Q is the activation energy for creep, R is the universal constant and n is the creep exponent. Creep rate data is obtained from Stephens and Klopp (Stephens and Klopp, n.d) and is fitted to Eq. (6). Table 1 lists creep law parameters for chromium.

3.1.4. Isotropic plasticity

For this study, plastic behavior is treated using an isotropic hardening model that is independent of, but used in conjunction with a creep model. This is done using a capability in MOOSE that permits the total inelastic strain to be expressed as a summation of contributions from an arbitrary number of inelastic models, and iteratively evaluates those models until they have converged. The plasticity model calculates the yield stress as a function of temperature and fluence. The yield strength can be expressed as a proof stress at 0.2% plastic deformation (between 300 and 1300 K) (Holzwarth and Stamm, 2002):

$$\sigma_{0.2} = (-8.24 \times 10^{-7}T^3 + 0.0019T^2 - 1.39T + 513.17)\text{MPa} \quad (7)$$

3.1.5. Irradiation hardening

Irradiation tests on pure chromium are extremely limited. A search for data on neutron irradiation of pure chromium only yielded one paper published in the 60 s (Weaver, 1968). Although this provides a very limited set of data, it gives a first order approximation of the effect of neutron irradiation on chromium. Table 2 shows data obtained from Fig. 1 in the referred paper at 200 °C (Weaver, 1968).

As data is only provided for one fluence level, and it is limited to fast neutron fluence (>1 MeV), we cannot use the hardening factor directly as assuming a constant hardening rate would give rise to a hardening factor of 119× at an end of life fluence of $\sim 1 \times 10^{26}$ n/m^2, which is clearly unreasonable. Therefore, examining results for other metals, such as FeCrAl (Pint et al., 2013), a rough estimate can be made that Cr will harden by at least 1.5× at end of life. Therefore, pending the availability of more experimental data, assuming end of life fluence of 10^{26} n/m^2, we use the following correlation:

$$\text{Irr}_{\text{factor}} = 5 \times 10^{-27}\phi + 1 \quad (8)$$

where ϕ is the fluence in n/m^2. Eq. (7) for yield strength can now be modified as follows:

$$\sigma_{\text{Irradiated}} = \sigma_{0.2} \times \text{Irr}_{\text{factor}} = \sigma_{0.2}(5 \times 10^{-27}\phi + 1)\text{MPa} \quad (9)$$

3.1.6. Oxidation and corrosion

At PWR steady state conditions, tests conducted by AREVA at 360 °C with simulated PWR chemistry showed negligible weight gain on the order of 1 mg/dm^2 after 180 days of exposure (Bischoff et al., 2016). This is consistent with recent findings by Ševeček et al. (Ševeček et al., 2018), where pure chromium samples had a negligible weight gain of 2.43 mg/dm^2 after 20 days of exposure at 500 °C. Therefore, corrosion at PWR steady state conditions will not be included in this work. As for oxidation behavior at high temperatures (>1000 °C), data is currently very limited as experimental efforts are still ongoing. Brachet et al. (Brachet et al., 2017) conducted one-sided steam oxidation test at 1200 °C. Their experiments showed the weight gain for the Cr-coated M5 to be ~15–20 times less than the uncoated material. Hyun-Gil Kim et al. (Kim et al., 2016) also conducted high temperature oxidation of Cr at 1200 °C and showed a 20-fold decrease in weight gain in comparison to uncoated Zr4. For the purpose of simplification and due to data limitations, we simply modify the parabolic rate law for zirconium with a reduction factor of 15 times in weight gain, and adopt that model for high temperature Cr oxidation. For the temperature range 673–1800 K, the Leistikov (Leistikow et al., 1983) correlation is used in BISON (Hales et al., 2016); this modification gives us:

$$(w_g)^2 = \left[2.33 \times 10^{-3}.\exp\left(\frac{20,962}{T}\right)\right].t(\text{g.cm}^{-2})^2 \quad (10)$$

where w_g is the weight gain in (g.cm^{-2}), t is time in seconds and T is the temperature in Kelvins. Taking the square root of Eq. (10) gives:

$$w_g = \left[4.83 \times 10^{-2}.\exp\left(\frac{10,481}{T}\right)\right].t^{\frac{1}{2}}(\text{g.cm}^{-2}) \quad (11)$$

A conversion factor of $2.22 \times 10^3 \mu$m.(cm^2.g^{-1}) is adopted from Lillerud et al. (Lillerud, 1980) to convert the weight gain to oxide thickness for chromium.

Table 1
Parameters of the creep law for chromium.

A [Pa^{-1}S^{-1}]	3.2555×10^{-40}
Q [J.mol^{-1}]	306268.8
R [J.mol$^{-1}K^{-1}$]	8.3145
n	6.2

Table 2
Irradiation Hardening for neutron irradiated Chromium.

Fluence [n/m^2]	Yield Strength [MPa]	Hardening Factor
0	144	1
2×10^{23}	179	1.238095

3.2. Silicon Carbide

In this section, we will list thermal and mechanical properties of SiC/SiC CVI (Chemical Vapor Infiltrated) ceramic matrix composite (CMC). Properties are adopted mainly from Stone et al. (Stone et al., 2015).

3.2.1. Thermal properties

The specific heat for composite SiC can be expressed as (Snead et al., 2007) (between 200 and 2400 K):

$$C_p(T) = 925.62 + 0.38T - 7.93 \times 10^{-5}T^2 - \frac{3.20 \times 10^7}{T^2}(\text{J} \cdot \text{kg}^{-1}\text{K}^{-1}) \quad (12)$$

Thermal conductivity for SiC/SiC is affected by neutron irradiation (Katoh et al., 2014). We will start first by listing unirradiated behavior and follow by discussing irradiation effects on conductivity. Unirradiated thermal conductivity is obtained from the following correlations (Stone et al., 2015; Snead et al., 2007; Deck et al., 2012):

$$K = -1.71 \times 10^{-11}T^4 + 7.35 \times 10^{-8}T^3 - 1.10 \times 10^{-4}T^2 + 0.061T + 7.97(\text{Wm}^{-1}\text{K}^{-1}) \quad (13)$$

The effect of irradiation on conductivity can be described by the defect thermal resistivity model proposed by Snead et al. (Snead et al., 2005):

$$K_{irr}^{-1} = K_0^{-1} + K_{rd}^{-1} \quad (14)$$

where K_{irr}^{-1} and K_0^{-1} are irradiated and unirradiated thermal resistivity. K_{rd}^{-1} is thermal resistivity from irradiation and can be expressed as (Snead et al., 2007; Katoh et al., 2014):

$$K_{rd}^{-1} = 15.11 \times S(Wm^{-1}K^{-1})^{-1} \quad (15)$$

where S is the volumetric swelling strain ($\Delta V/V_0$), which is described in the following section.

3.2.2. Mechanical properties

The elastic modulus exhibits a minor decrease with swelling (Katoh et al., 2014), while the Poisson's ratio is taken as a constant (Table 3).

The instantaneous coefficient of thermal expansion for SiC/SiC can be calculated using the following correlation (Katoh et al., 2014):

$$\alpha(T) = (3.83 \times 10^{-9}T^3 - 1.22 \times 10^{-5}T^2 + 0.0144T - 0.777) \times 10^{-6}(m.m^{-1}) \quad (16)$$

3.2.3. Volumetric swelling

Irradiation induced swelling in CVD SiC is described with the following equation from Katoh et al. (Katoh et al., 2013):

$$\dot{S} = k_s \gamma^{-1/3} \exp\left(-\frac{\gamma}{\gamma_{sc}}\right) \quad (17)$$

where $\dot{S}$ is the swelling rate, k_s is the rate constant for swelling, γ is the fast fluence (in dpa) and γ_{sc} is the characteristic fluence (in dpa) for swelling saturation by the negative feedback mechanism. The rate constant and characteristic saturation fluence can be described for the temperature range (473–1073 K) as follows:

$$k_s(T) = 0.10612 - 1.5904 \times 10^{-4}T + 6.0631 \times 10^{-8}T^2 \quad (18)$$

$$\gamma_{sc}(T) = 0.51801 - 2.7651 \times 10^{-3}T + 9.4807 \times 10^{-6}T^2 - 1.3095 \times 10^{-8}T^3 + 6.7221 \times 10^{-12}T^4(dpa) \quad (19)$$

with T in Kelvin. To convert fluence (n/m^2) into(dpa), a conversion factor of 10^{25} n/m2 (>0.1 MeV) per dpa is used (Katoh et al., 2014).

Although Eq. (19) has been shown to recreate experimental observations of neutron-induced swelling in SiC, it has been argued by Mieloszyk (Mieloszyk, 2015) to have two weaknesses when implemented in computer codes. First, it doesn't explicitly converge towards a saturation swelling. Second, it behaves erratically when integrated at low doses. For these aforementioned reasons, we adopt the Mieloszyk (Mieloszyk, 2015) numerical implementation to describe SiC swelling. The reader is referred to Section 7.2.2 in Mieloszyk (Mieloszyk, 2015) for detailed explanation of this implementation. The model is shown to predict expected swelling of SiC under variable temperature and dose history.

3.2.4. Pseudo-plasticity

The inter-woven nature of composite SiC/SiC allows it to deform in a pseudo-plastic manner, giving it an improved fracture toughness. Otherwise, SiC in general is treated as a purely linear-elastic material up to failure. The stress-strain behavior of SiC/SiC begins with a linear-elastic region up to the initiation of matrix cracking and then continues to deform non-linearly due to continuous matrix cracking and fiber sliding (Deck et al., 2012; Katoh et al., 2010). To account for this behavior a modified stress-strain curve is adopted as shown in Stone et al. (Stone et al., 2015). (ϵ_p, σ_p) are the proportional limit strain and stress respectively, where (ϵ_u, σ_u)refer to the ultimate tensile limit. These values are listed in Table 4 (Jacobsen et al., 2014). The stress-strain behavior is not significantly affected by either temperature up to 1000 °C (Lipetzky et al., 1996) or irradiation conditions in LWRs (Stone et al., 2015; Katoh et al., 2014); thus their effects are disregarded in this study.

For modeling implementation, this behavior can be represented by linking the Young's modulus to mechanical strain using the following correlation:

$$E = \begin{cases} 296 \times 10^9 Pa & \epsilon \leqslant \epsilon_p = 0.056\% \\ (5.5023 \times 10^{10}\epsilon + 1.3219 \times 10^8)/\epsilon & \epsilon > \epsilon_p = 0.056\% \end{cases} \quad (20)$$

3.2.5. Failure

Failure of SiC is statistical due to its brittle nature. It can be described using the Weibull model (Angelici Avincola et al., 2016):

$$P_f(\sigma) = 1 - \exp\left(-\left(\frac{\sigma - \sigma_c}{\sigma_0}\right)^m \frac{V}{V_0}\right) \quad (21)$$

where σ is the stress, σ_0 is the characteristic strength, σ_c is the stress below which no failure occurs, m is the Weibull modulus, V is the volume of the specimen and V_0 is the reference volume. The equation can be further simplified by assuming $(\sigma_c = 0)$ and $(V = V_0)$. This reduces to:

$$P_f(\sigma) = 1 - \exp\left(-\left(\frac{\sigma}{\sigma_0}\right)^m\right) \quad (22)$$

σ_0 and m are empirical parameters that are fitted experimentally. Table 5 lists values used for predicting failure probability for composite SiC (Angelici Avincola et al., 2016).

3.3. Zircaloy-4 and uranium dioxide

Thermo-mechanical properties for both Zircaloy-4 and standard UO_2 fuel are adopted as implemented in BISON with no modifications. The reader is referred to BISON's theory manual (Hales et al., 2016) for a detailed description of these properties. The BISON material models activated in each section will be listed in each's test description.

4. Steady-state simulations

4.1. Test description

A set of steady state simulations were designed to simulate representative US commercial PWR power plant operation (Andrews et al., 2016), with a total average fuel rod burnup of approximately ~60 MWd/kgU. These simulations included full-shutdown for all cases, to give an accurate representation of the cladding behavior and to account for the contribution of shutdown conditions to some phenomena such as pellet cladding mechanical interaction (PCMI) and swelling.

The model used is a 2D axisymmetric representation of a fuel rodlet with discrete fuel pellets. The rodlet is expected to produce similar behavior as the full length rod (Malik Wagih and Che,

Table 3
Elastic modulus and Poisson's ratio for SiC.

SiC/SiC	
Elastic modulus (GPa) Snead et al. (2007); Jacobsen et al. (2014)	296
Poisson's ratio Snead et al. (2007); Katoh et al. (2014)	0.18

Table 4
Mean stress-strain properties for SiC/SiC.

SiC/SiC	
Proportional limit stress (PLS) (σ_p)	163 MPa
Strain at PLS (ϵ_p)	0.056%
Ultimate tensile strength (σ_u)	404 MPa
Strain at UTS (ϵ_u)	0.494%

Table 5
Weibull failure model parameters.

	SiC/SiC
Weibull Characteristic Strength (σ_0)	290 MPa
Weibull Modulus (m)	17.5

2017). Details of the fuel rod geometry and specifications are summarized in Table 6. The cladding thicknesses were summarized in Section 2.1.

The power history for the steady state case is shown in Fig. 2, with a constant chopped-cosine shaped axial power profile with maximum peaking factor of 1.2 was used for the axial power profile. Other reactor operation parameters are tabulated in Table 7.

The 2-dimensional finite element mesh used quadratic finite elements with an axisymmetric formulation. The individual fuel pellets were meshed as discrete entities. Both the fuel and cladding used fine meshes, with 30 radial elements and 30 axial elements in each pellet. The cladding had 4 radial elements, and the number of axial elements were adjusted to provide approximately square elements for the cladding as shown in Fig. 3. The simulation for the reference Zircaloy-4 case had a total of 9612 elements.

For the fuel (UO_2), BISON's standard models were used to describe temperature and burnup dependent thermo-mechanical properties, fission product swelling, densification, thermal and irradiation creep with isotropic cracking, relocation, and fission gas production and release (Hales et al., 2016). For the base Zircaloy-4 cladding, BISON's standard material models were also used to describe temperature and burnup dependent mechanical properties, thermal and irradiation creep, and plasticity. Thermal conductivity of 16 W/m-K and heat capacity of 330 J/kg-K are used for the cladding.

4.2. Results

4.2.1. Zr4-based fuel system

The simulation results for the Zr4-Cr fuel system are shown in Figs. 4–10. The Zr4-Cr cladding showed comparable performance to the reference Zr4 cladding under steady-state operation. The reference Zr4 case with enhanced UO_2 is referred to as Zr4$*$ to differentiate from the other reference case, denoted as Zr4-ref as will be noted again in Section 4.2.2. Plenum pressure and fission gas released are slightly lower for the coated cladding as seen in Fig. 4. The major difference is the lower inward creep for the coated claddings, due to the higher stiffness of the coatings as well as lower thermal creep relative to Zircaloy-4. This results in delayed initiation of mechanical fuel/cladding contact as illustrated in Fig. 5. The slowed gap closure results in a slight difference in centerline fuel temperature for the first ~500 days of operation as shown in Fig. 6; the temperatures become similar after contact is achieved for the Zr4-Cr cladding as the metals have comparable thermal conductivity. As seen in Fig. 7, the coated claddings show slightly lower but comparable stresses in the base Zr4 layer, keeping it well below the plastic yield stress for Zr4. The stress and effective plastic strain for the Cr cladding is plotted in Fig. 8. The coating yields upon initial heating from room temperature, due to thermal mismatch with the base Zr4 layer. The coatings further yield to 1.3% plastic strain by the end of life. Chromium is expected to survive elongations of 40% before fracture at 300 °C (Holzwarth and Stamm, 2002) and thus is expected to survive the much lower 1.3% plastic strain experienced here without fracture. However, the expected plasticity warrants further experimental investigation of the cladding at these temperatures to test their integrity during operations.

Table 6
Steady state case Test rod specifications.

Fuel stack height	cm	15
Nominal Plenum height	cm	0.75348
Number of pellets per rod		15
Fill gas composition		He
Fill gas pressure	MPa	4.2
Fuel Enrichment	%	5
Density	%	95
Outer diameter	mm	8.1919
Grain diameter	μm	5
Pellet geometry		Dished
Dish spherical diameter	mm	21.2
Dish depth	mm	0.287
Chamfer width	mm	0.5
Chamfer depth	mm	0.16
Zr4-Cladding		
Outer diameter	mm	9.5
Inner diameter	mm	8.357
Wall thickness	mm	0.5715

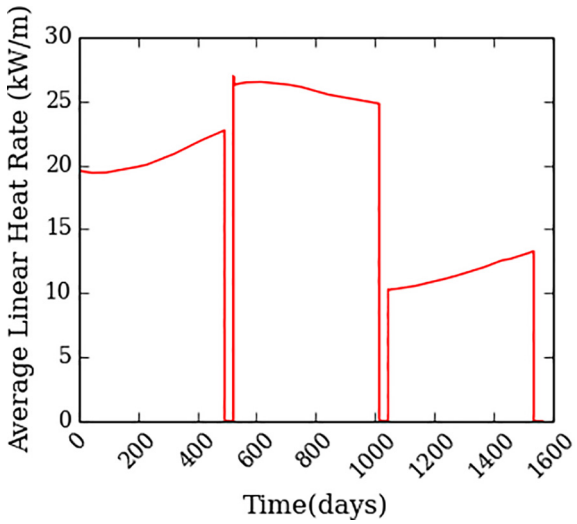

Fig. 2. BISON input power history for the steady state case.

Table 7
Operational input parameters.

Operational input parameters		
Coolant inlet temperature	C	293
Coolant pressure	MPa	15.5
Fast neutron flux	n/(cm^2.s)	4.022×10^{13}
Peaking factors	Chopped Cosine	

4.2.2. SiC-based fuel system

For the SiC-based fuel system, the reference Zr-4 case is different from the one used in the Zr4-based fuel system in Section 4.2.1. Using the same simulation conditions as the previous section resulted in significant pellet-clad contact pressures with the SiC/SiC-Cr cladding. This Pellet-Clad Mechanical Interaction (PCMI) occurred as a result of a significant increase in fuel temperature that promotes fuel swelling and relocation. The higher fuel temperature is due to a lack of cladding creep down (e.g. stiffer cladding) and lower cladding thermal conductivity compared to Zr4. However, this could also be due to some other aspect of the fuel swelling/relocation model implemented in BISON, as pellet-clad contact is not expected to occur with SiC based cladding based on predictions of the FRAPCON fuel performance code (Lee et al., 2013). In order to simplify matters and focus on the cladding behavior, we changed the UO_2 fuel thermal conductivity to 1.3 times the

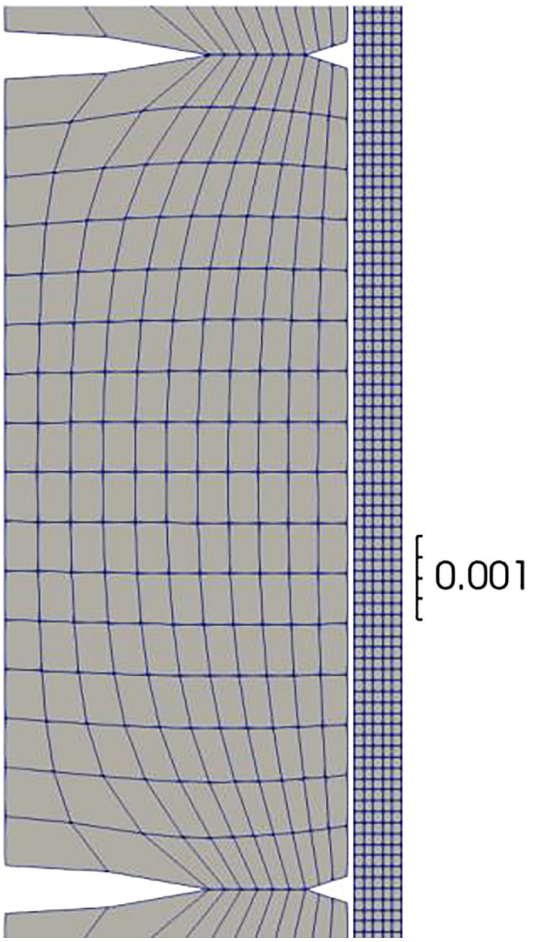

Fig. 3. Section of BISON mesh for the reference Zircaloy-4 case, scale is in meters.

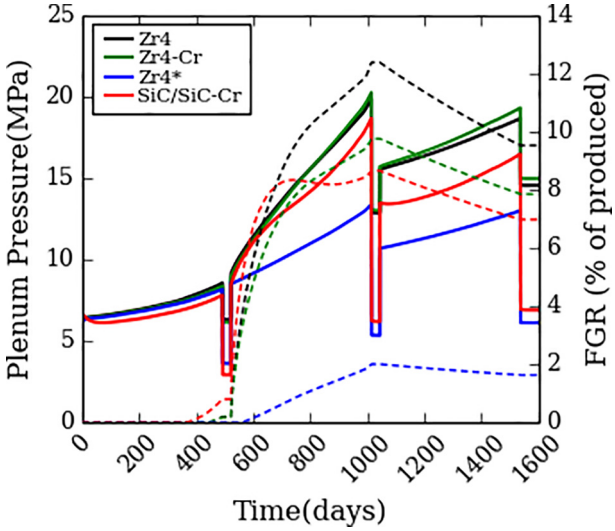

Fig. 4. Plenum pressure and fission gas released (FGR) under normal operation. (Solid – Left Axis; Dashed – Right Axis; Zr4*-Enhanced Fuel Conductivity).

implemented standard fuel conductivity in BISON. This can be thought of as enhancing the fuel conductivity using additives such as BeO, previously investigated to address the high fuel temperatures reached with SiC cladding (Sukjai, 2014). The idea is that pellet-clad contact should be avoided for SiC-based fuels by adjusting the design. The enhancement of the fuel conductivity by 1.3× resulted in much lower contact stresses for the SiC/SiC-Cr fuel. The reference Zr4 case in this section also has the enhanced fuel thermal conductivity for an unbiased comparison; thus the fuel centerline temperatures are expected to be lower than the reference Zr4 case in Section 4.2.1. The reference Zr4 case with enhanced UO_2 is referred to as Zr4∗ to differentiate from the other reference case, denoted as Zr4-Ref. Aside from the enhanced fuel conductivity, everything else is kept the same in the SiC/SiC-Cr simulations.

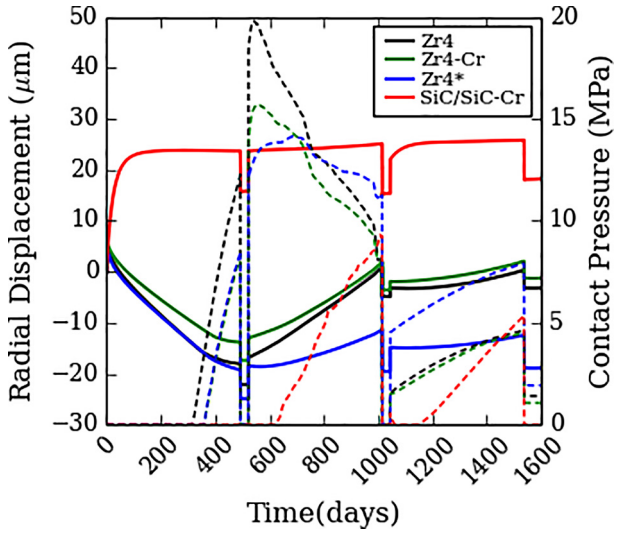

Fig. 5. Average cladding radial displacement and contact pressure under normal operation. (Solid – Left Axis; Dashed – Right Axis).

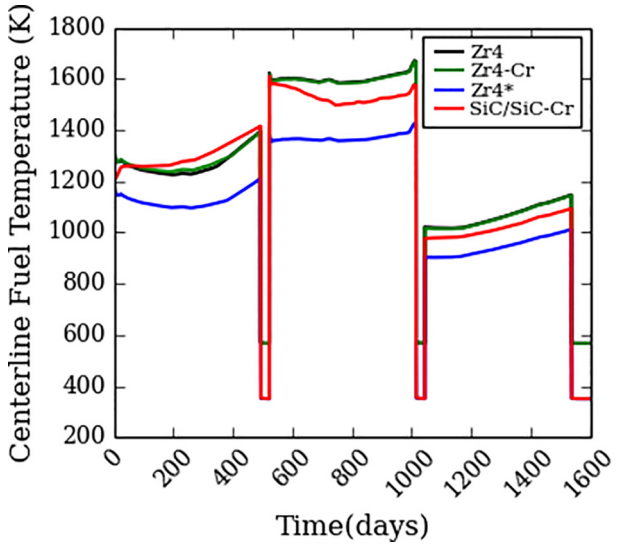

Fig. 6. Centerline fuel temperature under normal operation.

Looking at the results for the steady-state simulations, we can see that plenum pressure and fission gas release are higher for the SiC/SiC-Cr in comparison to the Zr4∗ reference case as seen in Fig. 4. This can be understood by looking at the calculated centerline fuel temperatures in Fig. 6, where the SiC/SiC-Cr fuel is ∼200 °C higher than reference Zr4∗; this is mainly due to the low thermal conductivity of SiC and lack of clad creep down. The higher temperatures result in more fission gas release and higher plenum pressures as well. Regarding the cladding radial displacement, the SiC/SiC-Cr cladding does not creep inwards like the Zr4∗ reference

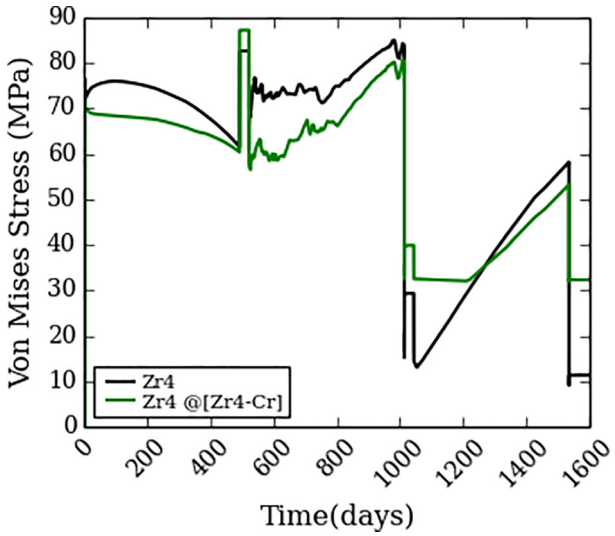

Fig. 7. Von Mises stresses in the base Zr4 cladding under normal operation.

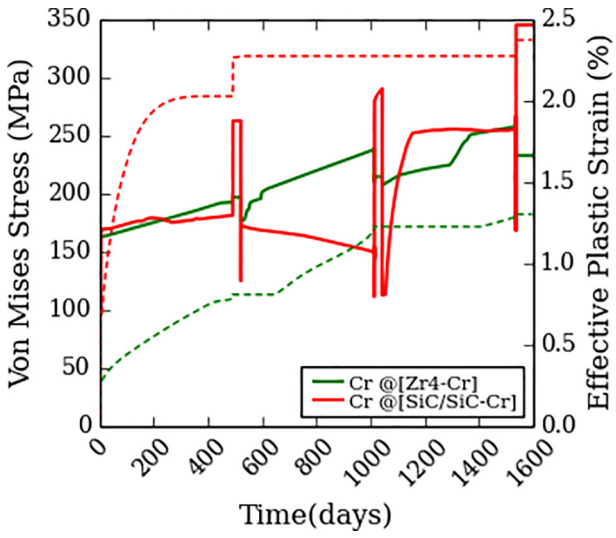

Fig. 8. Stresses and effective plastic strains of the Cr coatings under normal operation. (Solid- Left Axis; Dashed – Right Axis).

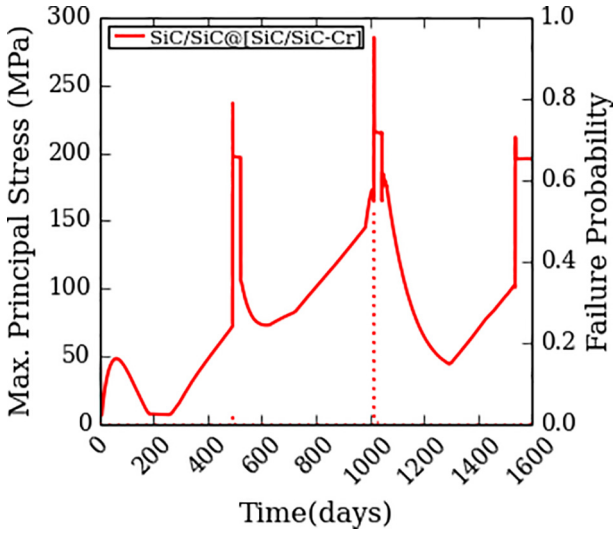

Fig. 9. Maximum principal stresses and failure probability for SiC/SiC layer under normal operation. (Solid – Left Axis; Dashed – Right Axis).

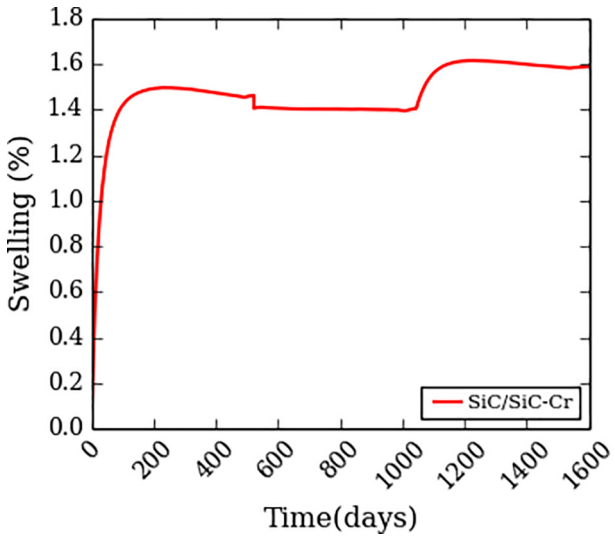

Fig. 10. Average swelling in SiC/SiC layer under normal operation.

case but rather keeps displacing outwards due to the irradiation induced swelling. Therefore, contact is delayed for the SiC/SiC-Cr cladding but still occurs. Fig. 9 shows the time history of the maximum principal stresses in the SiC layer, along with the failure probability indicated by the Weibull model, which reaches a maximum at the second shutdown of (P(f) = ~0.5). The higher stress at the second shutdown, in comparison to the first shutdown, could be the result of the pellet-clad contact occurring between the first and second shutdown. There is a potential for this pellet-clad interaction to be designed out by optimizing the gap thickness and cladding dimensions, and thus the SiC/SiC-Cr is still deemed promising for further investigation. It is worth noting that the Weibull model is used to compute a probability of failure given a single deterministically computed stress state. As the stress state is a function of a number of uncertain parameters, this should not be interpreted as accounting for the uncertainty in those parameters, which could be done using probabilistic sampling. The chromium coating is expected to yield up to an effective plastic strain of ~2.4%, which is higher than but still comparable to the Zr4-Cr fuel. It is expected that the Cr layer would be able to survive steady-state operation under these conditions.

5. Transient simulations: ramp test

5.1. Test description

To study the PCMI resistance of the proposed ATF concepts, they were subjected to a ramp test based on the French OSIRIS J12-5 test (IAEA, 2013). The experimental test was based on a segmented PWR rod that had been base-irradiated then re-fabricated and ramp-tested in the French Alternative Energies and Atomic Energy Commission (CEA) OSIRIS reactor. The rod simulated in the current work is a rodlet, represented using a 2D axisymmetric model with discrete fuel pellets. Details of the fuel rod geometry and specifications are summarized in Table 8. The coating thickness is kept at the same 50 μm thickness and is deducted from the thickness of the base Zr4 layer.

5.1.1. Operating conditions and irradiation history

Experimentally, the segmented Zr-4 rod was irradiated to a burnup of 23.852 MWd/kgU in the Electricity of France (EDF) Graveline 5 PWR. After base irradiation the rod-segment was re-

Table 8
Ramp case Test rod specifications.

Fuel		
Overall length	mm	522.4
Fuel stack height	mm	432.95
Nominal Plenum height	mm	89.44
Number of pellets per rod		32
Fill gas composition		He
Fill gas pressure	MPa	2.6
Fuel Enrichment	%	4.5
Density	%	95.73
Outer diameter	mm	8.192
Grain diameter	μm	10
Pellet geometry		Dished
Dish diameter	mm	6
Dish depth	mm	0.32
Zr4-Cladding		
Outer diameter	mm	9.5
Inner diameter	mm	8.36
Wall thickness	mm	0.57

fabricated with new end plugs, while retaining the fuel column and internal fill gas. The re-fabricated rod was then ramp-tested; first, the rod was reconditioned at 21 kW/m for 762 min, then the power was ramped at a rate of 9 kW/min up to 39.5 kW/m, where it was held for 739 min. The base-irradiation power history is shown in Fig. 11, and ramp test power history is shown in Fig. 12. The external clad temperature was estimated as a function of time as shown in Figs. 13 and 14. The axial peaking factor was kept flat at 1.0 for the base-irradiation run and changed to a constant cosine shaped peaking factor during the power ramp. The base power history and the power ramp is modified slightly by removing shutdown points, as it is not the focus of the section but rather the power ramp itself.

5.1.2. Geometry and mesh

The 2-dimensional finite element mesh used for these simulations used quadratic finite elements, with an axisymmetric formulation. The fuel pellets were modeled using discrete meshes. Both the fuel and cladding used medium-sized meshes. Each fuel pellet had 11 radial elements and 3 axial elements. The cladding and the coating had 4 and 2 radial elements respectively, and the number of axial elements were adjusted to have an axial/radial ratio of 4:1 approximately. The simulation for the reference Zircaloy-4 case had a total of 6704 elements.

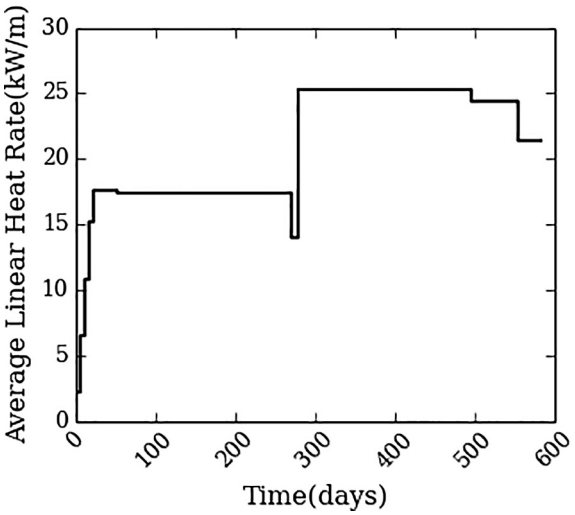

Fig. 11. BISON input power history for OSIRIS J12 in the Gravelines 5 PWR.

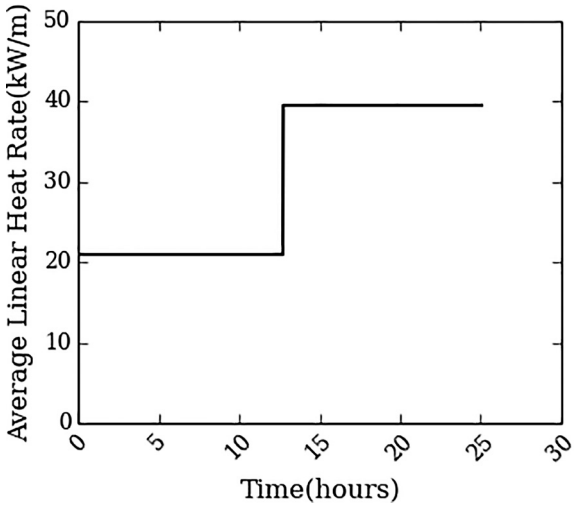

Fig. 12. BISON input power history for OSIRIS J12 power ramp test.

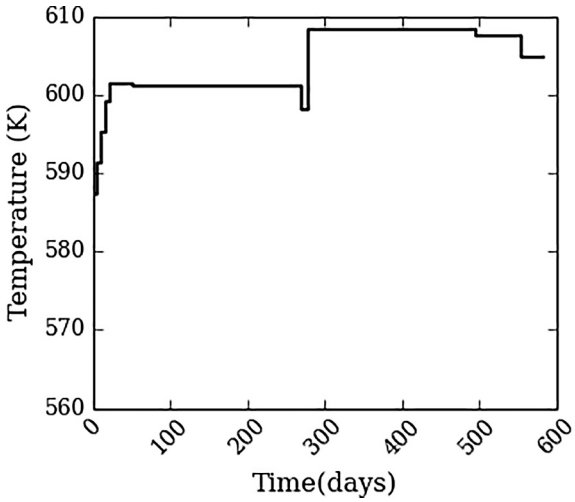

Fig. 13. External cladding temperature for OSIRIS J12 base-irradiation.

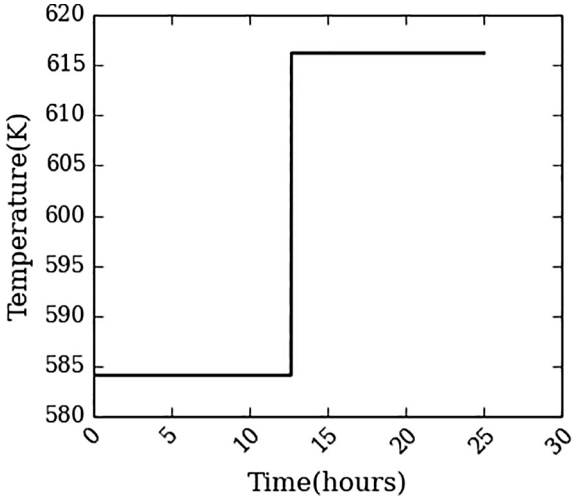

Fig. 14. External cladding temperature for OSIRIS J12 power ramp.

The UO_2 fuel is modeled as an elastic solid with the incremental finite strain formulation available in BISON. The Young's modulus is set to 200 GPa, the Poisson's ratio is 0.345, and the coefficient of thermal expansion is set to 10^{-5}. BISON's standard material models were used to describe temperature and burnup dependent thermo-mechanical properties, fission product swelling, densification, relocation, and fission gas production and release (Hales et al., 2016). The major difference from the models in Section 4.1 is the exclusion of models for fuel creep and isotropic cracking in this simulation for convergence reasons. For the base Zircaloy-4 cladding, the same BISON material models used in Section 4.1 were employed.

5.2. Results

5.2.1. Zr-based fuel systems

The results of the simulations are shown in Figs. 15–21. The power ramp simulations show similar trends to the steady-state scenarios shown earlier; these trends in the effect of cladding on plenum pressure, fission gas release, and centerline fuel temperatures for the Zr4-Cr cladding in comparison to the reference case can be seen in Figs. 15 and 17. Pellet-clad contact initiation is again delayed for the coated cladding as seen in Fig. 16, due to lower inward creep, resulting in lower contact pressures. The base Zr4 layer stress is almost reduced to half in the Cr-coated cladding as shown in Fig. 18. This is mainly due to the lower pellet-clad contact pressure. In the Cr coating, the stresses resulting from the power ramp are not high enough to cause any significant increase in plastic strains in comparison to pre-power ramp steady state levels of about 1% as seen in Fig. 19. It is important to note here that in all cases, the coating yields before the cladding. In this simulation, as the coatings had accumulated plasticity prior to the power ramp, it showed no further deformation when subjected to the power. We also considered a case where we subject a fresh fuel with zero fuel-clad gap to the 25 h power ramp, thus eliminating the base history irradiation done earlier. The results can be seen in Fig. 21, where the coating starts yielding as soon as the fuel pellet starts pushing against the cladding. Therefore, the coating plasticity is still an issue for power ramps with fresh fuel and should be further investigated. However, under normal conditions, it is expected that power ramps, which might occur in the fuels having burnups up to ~30 MWd/kgU, would have no significant impact on the coated Zr4-based cladding performance. In Section 6, we look at LOCA simulations to test the claddings under more extreme transients.

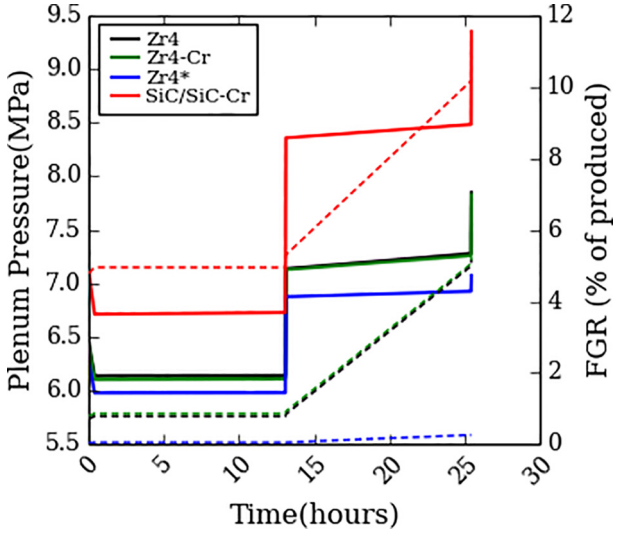

Fig. 15. Plenum pressure and fission gas released (FGR) under power ramp. (Solid – Left Axis; Dashed – Right Axis).

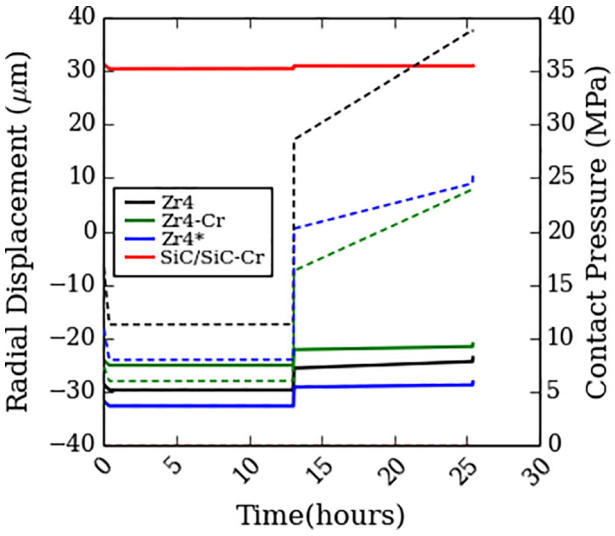

Fig. 16. Average cladding radial displacements and contact pressures under power ramp. (Solid – Left Axis; Dashed – Right Axis).

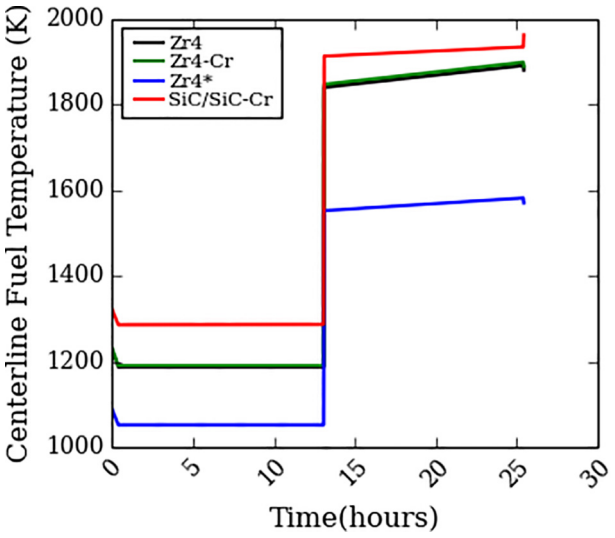

Fig. 17. Centerline fuel temperatures under a power ramp.

5.2.2. SiC-based fuel systems

The 1.3× thermal conductivity enhancement factor was used for the fuel as in Section 4.2.2; the reference case is again referred to as Zr4∗. Looking at Fig. 15, we can see higher calculated plenum pressures and fission gas release for the SiC/SiC-Cr fuel in comparison to the reference Zr4∗ case. This is expected due to the almost ~400 °C degrees difference in centerline fuel temperatures as seen in Fig. 17. However, in this simulation pellet-clad contact did not occur for the SiC/SiC-Cr cladding as seen in Fig. 16; this is because SiC-based claddings do not creep inwards like the Zr4∗ reference, but rather displace outwards due to the radiation induced swelling. The SiC/SiC-Cr cladding has a negligible failure probability, rising to a maximum of $(P(f) = 2.4 \times 10^{-11})$ and no increase in the Cr coating plastic strain due to the power ramp as seen in Fig. 19. The plastic strain hovers at around 1% at this point. Therefore, the SiC/SiC-Cr is expected to survive a power ramp of this scale.

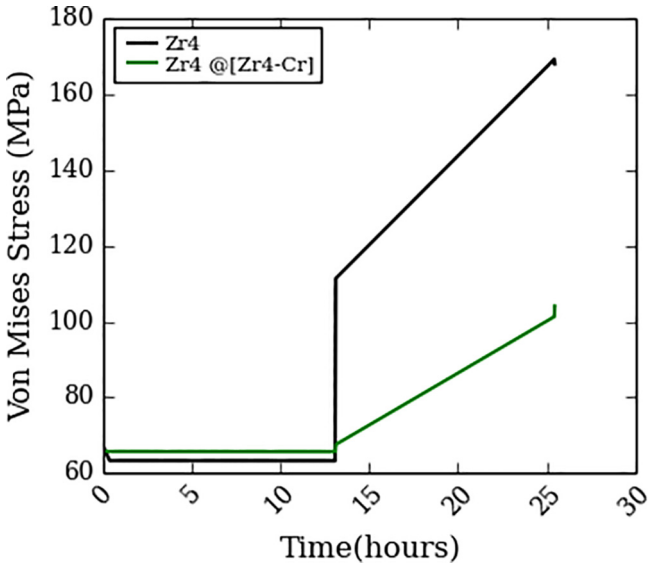

Fig. 18. Stresses in the base Zr4 layer for the Zr4-based fuels under a power ramp.

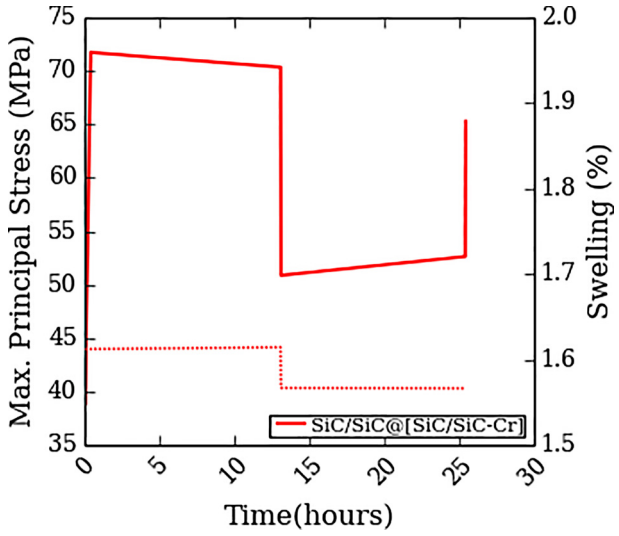

Fig. 20. Maximum principal stresses and swelling for SiC/SiC layer under power ramp.

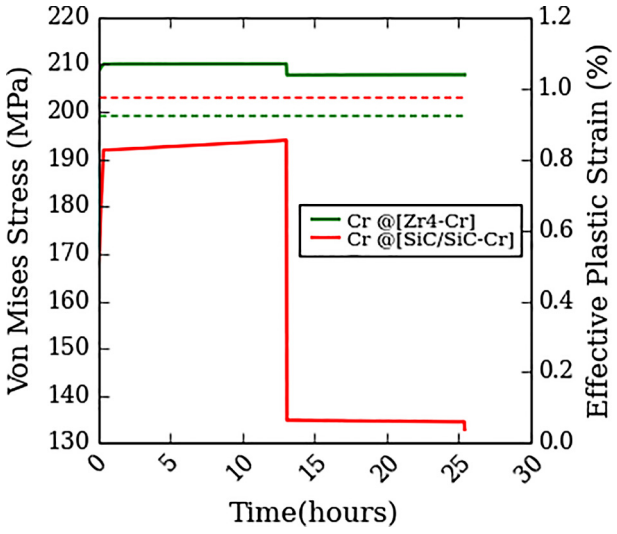

Fig. 19. Stresses and effective plastic strains of Cr coatings under a power ramp. (Solid – Left Axis; Dashed – Right Axis).

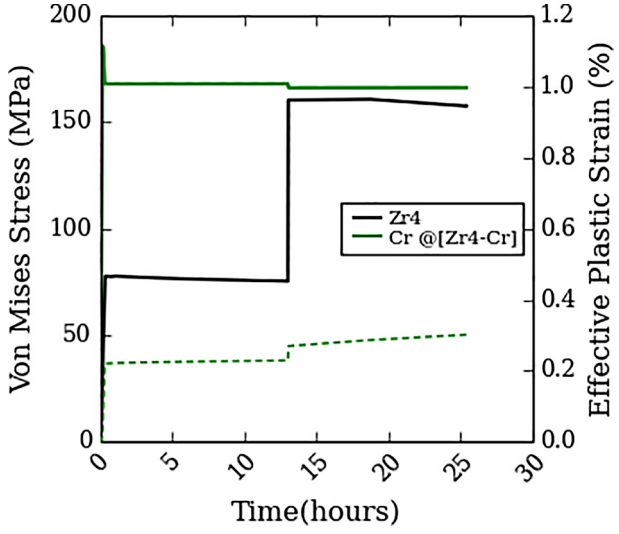

Fig. 21. Stresses and plastic deformation Cr Coating and base Zr4 for PCI of a fresh fuel with no pellet-clad gap. (Solid – Left Axis; Dashed – Right Axis).

6. Transient simulations: LOCA

6.1. Overview

To conclude the testing of the fuel concepts, LOCA fuel analysis simulations were carried out. To mirror experimental conditions, we chose the MT-4 test conducted in the National Research Universal (NRU) reactor at Chalk River National Laboratory in Canada by Pacific Northwest Laboratory (Wilson et al., 1993; P.C. by L Wilson et al., 1993). The tests were conducted under the LOCA simulation program sponsored by the US Nuclear Regulatory Commission (NRC). The experiments used full-length fuel rods, with test conditions designed to simulate adiabatic heat-up, re-flood and quench phases of a large-break LOCA.

6.2. Test description

The model represents a fuel rodlet with a smeared fuel column using a 2D axisymmetric representation. Details of the fuel rod geometry and specifications are summarized in Table 9. The Cr coating is kept at the same 50 μm thickness and is deducted from the base Zr4-cladding thickness.

6.2.1. Operating conditions and irradiation history

The test rods were irradiated in flowing steam prior to the transient, then kept in stagnant steam for the transient duration; at the end, re-flooding conditions are introduced to conclude the test. The re-flooding rate is averaged to 5 in/s (~0.127 m/s) in the BISON input. The test conditions are summarized in Table 10. The axial power profile uses a constant cosine shaped peaking factor. The pre-transient axial temperature profile follows the following correlation:

$$T(K) = -24.096y^2 + 152.47y + 437.81 \quad (23)$$

where y is the distance from the bottom of the clad.

During the experiments, the claddings generally failed during the adiabatic heat-up phase, prior to re-flooding. As we are interested in the failure behavior of the ATF concepts, we will focus

Table 9
LOCA case Test rod specifications.

Fuel		
Overall length	mm	3880
Fuel stack height	mm	3660
Nominal Plenum height	mm	200
Number of pellets per rod		1
Fill gas composition		He
Fill gas pressure	MPa	4.62
Enrichment	%	2.93
Density	%	95
Outer diameter	mm	8.26
Pellet geometry		Smeared
Grain diameter	μm	7.8
Zr4-Cladding		
Outer diameter	mm	9.63
Inner diameter	mm	8.41
Wall thickness	mm	0.61

Table 10
Operating conditions for the MT-4 LOCA test.

Power level	kW/m	1.2
Pre-transient cladding temperature	K	640
Pre-transient internal gas pressure	MPa	9.3
Steam pressure	MPa	0.28
Delay time before reflood	s	57
Reflood rate	in/s	8 in/s for 6 s 4 in/s for 6 s 1 in/s for 3 s
Reflood temperature	K	311

our analysis on the time required for failure in comparison to the reference Zr4 case.

To model a harsher LOCA case, the base irradiation was modified from the original experimental conditions. Prior to the LOCA transient, a steady state simulation was run with a straight power history of 20 kW/m of linear heat generation to mimic base irradiation run up to ~40 MWd/kgU. After that, the simulation case was restarted and subjected to the LOCA transient. Therefore, the LOCA is modeled is to occur after a burnup of ~40 MWd/kgU rather than the nearly fresh fuel conditions of the experiments. The steady state run will cause accumulation of stresses, strains and coating plasticity prior to the LOCA transient.

6.2.2. Geometry and mesh

As for the previous cases, a 2-dimensional finite element model with an axisymmetric formulation and quadratic finite elements was used in the simulations. The fuel pellets were modeled as a single smeared fuel column. The fuel, cladding and coating had 12, 4 and 2 radial elements respectively. The simulation for the reference Zirc-4 case had a total of 1900 elements. Axially, the elements had a ratio of ~5:1.

The UO_2 fuel was modeled as described in Section 5.1.2. The base Zr4 cladding was modeled as an elastic solid with an incremental finite strain formulation. The Young's modulus is set to 75 GPa, the Poisson's ratio is 0.3, and a constant coefficient of thermal expansion of 5×10^{-6} is used. A thermal conductivity of 16 W/m-K and heat capacity of 330 J/kg-K are used. Standard BISON material models are used to describe LOCA large deformation creep, which is activated above 900 K, phase transformation of Zr alloy from hexagonal (α-phase) to cubic (β-phase) crystal structure under high-temperature conditions, and finally cladding failure due to burst of Zircaloy-4 during LOCA accidents (Hales et al., 2016).

6.3. Results

6.3.1. Zr-based fuel systems

The results of the LOCA simulations are shown in Figs. 22–26. The time to rupture, maximum rupture hoop strain, average cladding temperature and the rod pressure at rupture are summarized for the Zr4-based fuels in Table 11. For this simulation, both creep and plasticity were included for the coatings. The time to failure of Zr4-Cr is slightly lower than, but still close, to the reference Zr-4 case. This could be the result of reduced thickness of the base Zr4 cladding, which carries the bulk of the structural load. This might be slightly improved by adjusting the thickness of the Cr coating, but in general it seems the difference in time to failure is limited to few seconds. The two claddings failed before reflooding which is introduced after 60 s of the test.

The two claddings showed ballooning behavior at the midsection as shown in Figs. 23 and 26. The burst location is located at the site with maximum displacement in each case. The key finding from these analyses was that the Cr-coated cladding showed comparable performance to the non-coated cladding for the LOCA conditions. While chromium is highly ductile, experimental work is required to confirm these findings for these conditions as it is could be possible that the coatings will not survive the extensive plastic deformation (~13%) experienced, as shown in Fig. 22. It is also worth noting that the coating also experienced a maximum creep strain magnitude of 0.4%. As this is much lower in magnitude than the plastic deformation, the plastic strain is the primary concern. In the meantime, however, it is reasonable to assume that the coatings will provide performance that is at least comparable to the reference Zr4 cladding. Consistent with this assumption, Brachet et al. (2018) reported a slightly higher temperature to rupture for the Cr-coated cladding, as well as a reduction of the balloon size and rupture opening in comparison to the uncoated cladding.

6.3.2. SiC-based fuel systems

The SiC-based were subjected to the same LOCA scenarios. The enhanced fuel thermal conductivity (1.3x) was again used to be consistent with the steady state and power ramp simulations. The Zr4∗ reference case results are listed Table 11. Looking at Fig. 24, the SiC/SiC-Cr cladding shows a very low (max P(f) = 0.0036) failure probability. The resulting hoop strains shown in

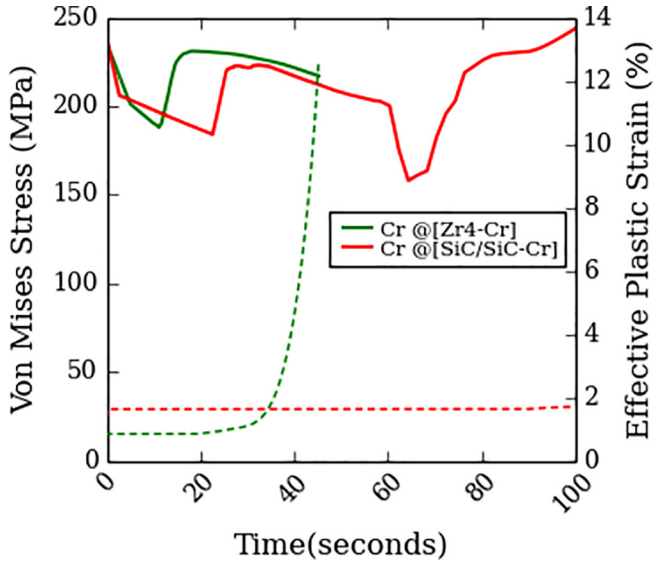

Fig. 22. Stresses and effective plastic strain of Cr coatings during MT-4 LOCA. (Solid – Left Axis; Dashed – Right Axis).

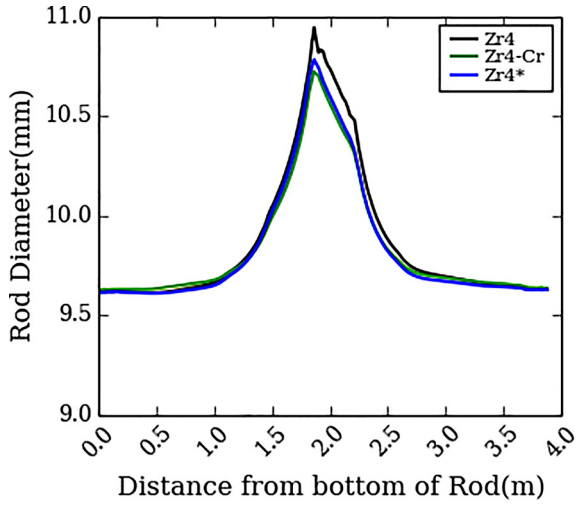

Fig. 23. Cladding dimensions at burst showing ballooning at the mid-section.

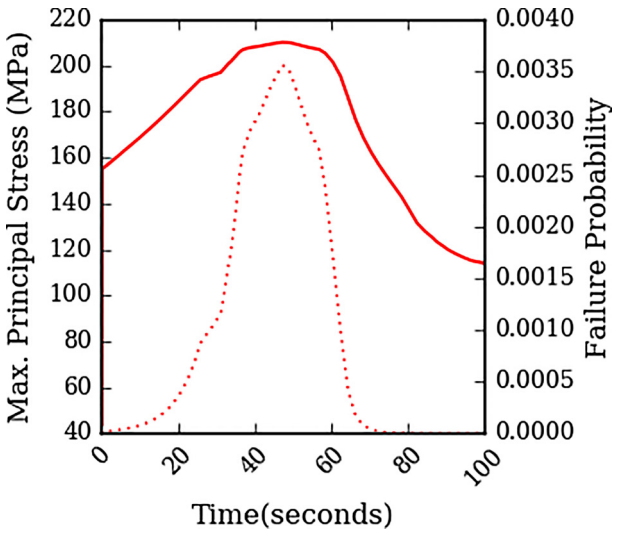

Fig. 24. Maximum principal stress and failure probability for the SiC layer during MT-4 LOCA.

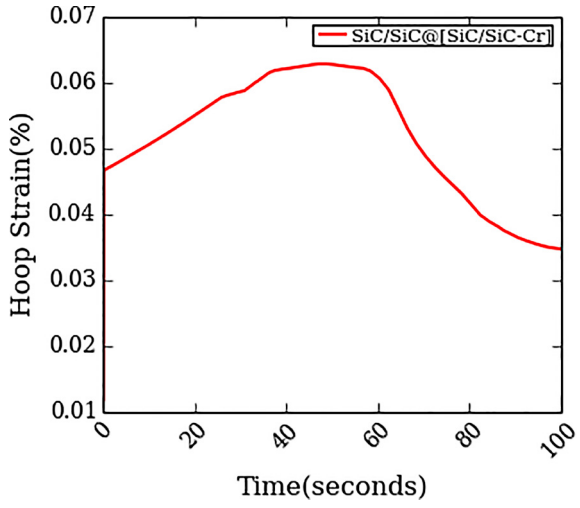

Fig. 25. Hoop Strain of SiC/SiC layer during MT-4 LOCA.

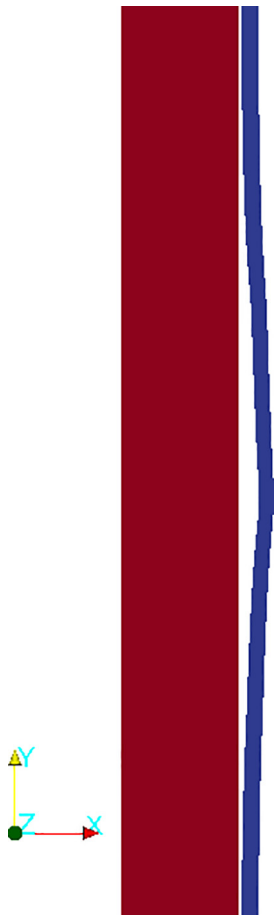

Fig. 26. Sectional view of ballooning at mid-section (x-axis is scaled 50:1).

Fig. 25 puts the SiC/SiC layer in SiC/SiC-Cr slightly above the strain at the proportional limit stress (~0.056%), but are still much lower than the strain at ultimate tensile strength (0.494%) (Stone et al., 2015). The plastic strain in the Cr coating is kept at ~1.8% which matches earlier strains from the steady-state operation. The SiC/SiC-Cr fuel system is shown to survive LOCA, both the heating and re-flooding phase unlike the Zr4-based claddings in Section 6.3.1, where both layers failed just prior to re-flooding. Therefore, SiC-based fuels might prove more advantageous in more extreme conditions like LOCA, in terms of survival and expected coating deformations. However, it is important to note that the current modeling approach neglects the potential annealing of the radiation-induced swelling in the SiC/SiC composite material in lieu of lack of proper experimental data (Price, 1977; Ferguson, 1967). The inclusion of such physics could have substantial impact on the stress/strain evolution of SiC/SiC during such accident.

7. Parameter study

The results in the paper depend on the validity of implemented material properties of chromium. Experimental efforts is still needed to improve the quality of the data and provide neutron-irradiated properties in the future. Given the limited data that the models are based on, it is important to understand the sensitivity to these highly uncertain model parameters. In this section we perform a simple study on the effect of varying three different parameters in comparison to the Zr4-Cr case reported in the steady state simulation section (4.2.1). The two material properties with

Table 11
Simulation results for the MT-4 LOCA test.

		Zr4	Zr4-Cr	Zr4*
Time to Rod Rupture	s	47.5738	45.2281	44.0869
Maximum Hoop Strain	%	14.97	13.14	13.70
Rod Pressure at Rupture	MPa	9.00	10.11	8.95
Peak Cladding Temperature	K	1027.72	1037.14	1033.02

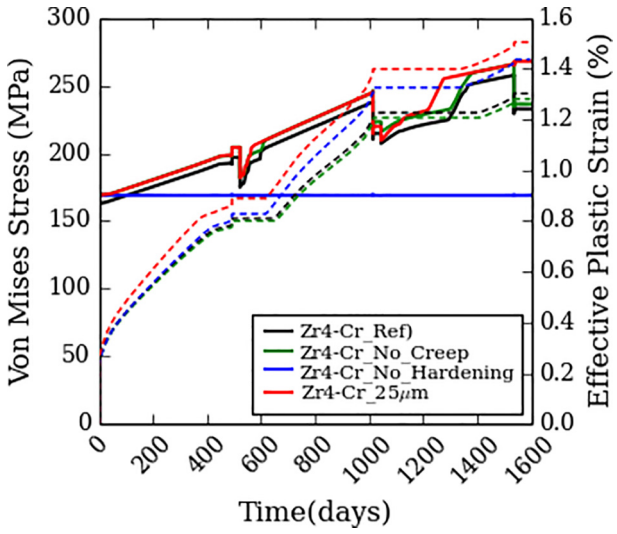

Fig. 27. Sensitivity analysis for the Cr Coating under steady state operating conditions. (Solid – Left Axis; Dashed – Right Axis).

very limited data reported earlier (Section 3.1) were Cr thermal creep and irradiation hardening. To understand the effects of creep and irradiation hardening, simulations were run with no creep and no irradiation hardening, and are shown as part of the set of results of this parameter study in Fig. 27.

As chromium creep is expected to be very low under these conditions, the case without creep was very similar to the reference case with insignificant difference in stresses and end of life coating plastic strain (less than ~2% difference). As would be expected, the case without hardening maintained a constant von Mises stress throughout operation, equivalent to the yield stress at that temperature. The end-of-life plastic strain was 10% higher than the reference case. Therefore, the irradiation hardening parameter is somewhat important to having a correct estimation of deformation during operation.

In addition, a case with reduced coating thickness of 25 μm Cr was simulated. As shown in Fig. 27, the 25 μm case had slightly higher stresses than the reference 50 μm case, and had a 16% higher end-of life plastic strain (1.5% in magnitude). The magnitude of the plastic strain is still under 2%, which indicates that the coating is expected to survive steady state conditions. This initial result shows that a coating as thin as 25 μm could be viable, pending further investigation under transient conditions. Future work should include optimization of the thickness from economic, neutronic and structural perspectives informed by the particular fabrication technology.

8. Conclusion

This paper investigated two potential ATFs, one Zr4-based fuel system (Zr4-Cr) and one SiC based fuel system (SiC/SiC-Cr). The proposed fuel systems were tested under PWR steady-state operation conditions, power ramps and finally LOCA transients. The following is a summary of the findings for each proposed fuel system:

- **Zr4-Cr:** This cladding showed promising performance under steady-state, power ramp cases and LOCA. While chromium is highly ductile, elongating up to 40% before fracture (Holzwarth and Stamm, 2002), any plastic strain can be detrimental to its performance and requires more experimental investigation of this condition. Furthermore, future modeling should consider damage and possible fracture. In general, the Zr4-Cr fuel concept seems to be promising for further investigation.
- **SiC/SiC-Cr:** The chromium coated composite SiC fuel showed promising results under both power ramps and LOCA transients; steady state operation shows high contact pressures that result in a high failure probability of ~0.5. However, the SiC/SiC-Cr is shown to survive shutdown (first shutdown), which was the source of failure in previous investigations of SiC claddings (Stone et al., 2015; Angelici Avincola et al., 2016). If pellet/-cladding contact can be avoided completely by optimizing the gap thickness or improving fuel/cladding thermal conductivity, the SiC/SiC-Cr is expected to survive normal operation. For the power ramps and LOCA, the failure probability was calculated to be small with a maximum of ~0.0036 in the LOCA. The plastic deformation of the chromium coating in steady state and power ramps was comparable to Zr4-Cr fuel, reaching up to ~2.5% plastic strains. However, the SiC/SiC-Cr shows a clear advantage under LOCA conditions, since no burst is predicted. This kept the Cr layer plastic strain below 2% in comparison to the 13% reached in the Zr4-Cr fuel. This could be explained by the higher stiffness of SiC/SiC in comparison to the base Zr4 layer, thus causing lower strains in the Cr coating under the same pressures and conditions. It should be noted that the current analysis neglects the high temperature annealing of SiC/SiC irradiation induced swelling during LOCA due to scarcity of data (Snead et al., 2018). In general, these analyses indicate that the SiC/SiC-Cr is a promising concept and should be further investigated.

In conclusion, both of the chromium-coated fuel systems investigated here seem to be promising ATF concepts. Both concepts had comparable performance to the reference Zircalloy-4 design in all three simulation scenarios. As we expect the Cr coatings to provide an order of magnitude improvement in oxidation resistance (Brachet et al., 2017; Kim et al., 2016), the two fuels should be further investigated experimentally as well as possible modeling of beyond design-basis accidents. In addition, the resulting plastic strains in the coatings indicate that future work should include consideration of damage and fracture.

Acknowledgements

Financial support for this work was provided by the US Department of Energy Integrated Research Project Grant # DE-NE0008416. The authors would like to thank Yifeng Che for her help setting up the mesh files for multi-layered claddings.

References

Andrews, N., Shirvan, K., Pilat, E.E., Kazimi, M.S., 2016. Steady State and Accident Transient Analysis Burning Weapons-Grade Plutonium in Thorium and Uranium with Silicon Carbide Cladding. Nucl. Technol. 194, 204–216. https://doi.org/10.13182/NT15-41.

Angelici Avincola, V., Guenoun, P., Shirvan, K., 2016. Mechanical performance of SiC three-layer cladding in PWRs. Nucl. Eng. Des. 310, 280–294. https://doi.org/10.1016/J.NUCENGDES.2016.10.008.

Armstrong Harry, P.E., 1964. Volume 230 – Institute of Metals Division – Dynamic Young's Modulus Measurements above 1000°C on Some Pure Polycrystalline Metals and Commercial Graphites. Trans. Metall. Soc. AIME. 230, 962–966. http://www.onemine.org/document/document.cfm?docid=25617 (accessed August 6, 2017).

Bischoff, J., Vauglin, C., Delafoy, C., Barberis, P., Perche, D., Guerin, B., Vassault, J., 2016. Development of Cr-coated Zirconium Alloy Cladding for Enhanced Accident Tolerance. In: Top Fuel 2016. pp. 1165–1171.

Brachet, J.C., Lorrette, C., Michaux, A., Sauder, C., Idarraga-Trujillo, I., Le Saux, M., Le Flem, M., Schuster, F., Billard, A., Monsifrot, E., Torres, E., Rebillat, F., Bischoff, J., Ambard, A., 2014. CEA studies on advanced nuclear fuel claddings for enhanced Accident Tolerant LWRs Fuel(LOCA and beyond LOCA conditions). In: FONTEVRAUD 8- Contrib. Mater. Investig. Oper. Exp. to LWRs' Safety, Perform. Reliab, pp. 10. doi:10.13140/2.1.5105.6325.

Brachet, J.-C., Le Saux, M., Le Flem, M., Urvoy, S., Rouesne, E., Guilbert, T., Cobac, C., Lahogue, F., Rousselot, J., Tupin, M., Billaud, P., Hossepied, C., Schuster, F., Lomello, F., Billard, A., Velisa, G., Monsifrot, E., Bischoff, J., Ambard, A., 2015. On-going studies at cea on chromium coated zirconium based nuclear fuel claddings for enhanced accident tolerant lwrs fuel. In: Top Fuel.

Brachet, J.C., Dumerval, M., Lezaud-Chaillioux, V., Le Saux, M., Rouesne, E., Hamon, D., Urvoy, S., Guilbert, T., Houmaire, Q., Cobac, C., Nony, G., Rousselot, J., Lomello, F., Schuster, F., Palancher, H., Bischoff, J., Pouillier, E., 2017. Behavior of Chromium Coated M5 Claddings under LOCA Conditions. In: 2017 Water React. Fuel Perform. Meet. 2017 Water React. Fuel Perform. Meet., pp. 1–11.

Brachet, J.C., Le Saux, M., Lezaud-Chaillious, V., Dumerval, M., Houmaire, Q., Lomello, F., Schuster, F., Monsifrot, E., Bischoff, J., Pouiller EdF, E.R. Behavior Under Loca Conditions Of Enhanced Accident Tolerant Chromium Coated Zircaloy-4 Claddings, (n.d.). https://www.researchgate.net/profile/Jean-Christophe_Brachet/publication/308097940_Behavior_under_LOCA_conditions_of_Enhanced_Accident_Tolerant_Chromium_Coated_Zircaloy-4_Claddings/links/57d9a58808ae0c0081efb835/Behavior-under-LOCA-conditions-of-Enhanced- (accessed February 14, 2018).

Carmack, J., Goldner, F., Bragg-Sitton, S.M., Snead, L.L., 2013. Overview of the U.S. DOE Accident Tolerant Fuel Development Program. https://inldigitallibrary.inl.gov/sites/sti/sti/6013242.pdf (accessed October 12, 2017).

Cheng, B., Kim, Y.-J., Chou, P., 2016. Improving accident tolerance of nuclear fuel with coated mo-alloy cladding. Nucl. Eng. Technol. 48, 16–25. https://doi.org/10.1016/J.NET.2015.12.003.

Deck, C.P., Khalifa, H.E., Back, C.A., 2012. Effects of structure and processing on the thermal conductivity of SiC-SiC composites. In: Trans. Am. Nucl. Soc. pp. 1123–1125. http://www.scopus.com.

Deck, C.P., Khalifa, H.E., Sammuli, B., Hilsabeck, T., Back, C.A., 2012. Fabrication of SiC-SiC composites for fuel cladding in advanced reactor designs. In: Prog. Nucl. Energy, Pergamon, pp. 38–45. doi:10.1016/j.pnucene.2011.10.002.

Deck, C.P., Jacobsen, G.M., Sheeder, J., Gutierrez, O., Zhang, J., Stone, J., Khalifa, H.E., Back, C.A., 2015. Characterization of SiC–SiC composites for accident tolerant fuel cladding. J. Nucl. Mater. 466, 667–681. https://doi.org/10.1016/J.JNUCMAT.2015.08.020.

Ferguson, I.F., 1967. Lattice contractions associated with the neutron irradiation of self-bonded silicon carbide. Philos. Mag. 16, 635–636. https://doi.org/10.1080/14786436708220870.

Field, K.G., Briggs, S.A., Sridharan, K., Howard, R.H., Yamamoto, Y., 2017. Mechanical properties of neutron-irradiated model and commercial FeCrAl alloys. J. Nucl. Mater. 489, 118–128. https://doi.org/10.1016/J.JNUCMAT.2017.03.038.

Field, K.G., Briggs, S.A., Edmondson, P., Hu, X., Littrell, K.C., Howard, R., Parish, C.M., Yamamoto, Y., 2015. Evaluation on the Effect of Composition on Radiation Hardening and Embrittlement in Model FeCrAl Alloys.

Galloway, J., Unal, C., 2016. Accident-Tolerant-Fuel Performance Analysis of APMT Steel Clad/UO_2 Fuel and APMT Steel Clad/UN-U_3Si_5 Fuel Concepts. Nucl. Sci. Eng. 182, 523–537. https://doi.org/10.13182/NSE15-7.

Gamble, K.A., Barani, T., Pizzocri, D., Hales, J.D., Terrani, K.A., Pastore, G., 2017. An investigation of FeCrAl cladding behavior under normal operating and loss of coolant conditions. J. Nucl. Mater. 491, 55–66. https://doi.org/10.1016/J.JNUCMAT.2017.04.039.

Gaston, D., Newman, C., Hansen, G., Lebrun-Grandié, D., 2009. MOOSE: A parallel computational framework for coupled systems of nonlinear equations. Nucl. Eng. Des. 239, 1768–1778. https://doi.org/10.1016/j.nucengdes.2009.05.021.

Hales, J.D., Williamson, R.L., Novascone, S.R., Pastore, G., Spencer, B.W., Stafford, D.S., Gamble, K.A., Perez, D.M., Liu, W., 2016. BISON Theory Manual The Equations behind Nuclear Fuel Analysis. doi:10.2172/1374503.

Holzwarth, U., Stamm, H., 2002. Mechanical and thermomechanical properties of commercially pure chromium and chromium alloys. J. Nucl. Mater. 300, 161–177. https://doi.org/10.1016/S0022-3115(01)00745-0.

Huenteler, J., Schmidt, T.S., Kanie, N., 2012. Japan's post-Fukushima challenge – implications from the German experience on renewable energy policy. Energy Policy 45, 6–11. https://doi.org/10.1016/j.enpol.2012.02.041.

IAEA, Improvement of Computer Codes Used for Fuel Behaviour Simulation (FUMEX–III), 2013. http://www-pub.iaea.org/MTCD/Publications/PDF/TE-1697_CD/PDF/IAEA-TECDOC-1697.pdf (accessed November 3, 2017).

Jacobsen, G.M., Stone, J.D., Khalifa, H.E., Deck, C.P., Back, C.A., 2014. Investigation of the C-ring test for measuring hoop tensile strength of nuclear grade ceramic composites. J. Nucl. Mater. 452, 125–132. https://doi.org/10.1016/j.jnucmat.2014.05.002.

Jorant, C., 2011. The implications of Fukushima. Bull. At. Sci. 67, 14–17. https://doi.org/10.1177/0096340211414842.

Katoh, Y., Ang, C., Linton, K., Terrani, K., Carpenter, D., 2017. In-pile Hydrothermal Corrosion Evaluation of Coated SiC Ceramics and Composites. https://info.ornl.gov/sites/publications/Files/Pub103017.pdf (accessed February 14, 2018).

Katoh, Y., Snead, L.L., Nozawa, T., Kondo, S., Busby, J.T., 2010. Thermophysical and mechanical properties of near-stoichiometric fiber CVI SiC/SiC composites after neutron irradiation at elevated temperatures. J. Nucl. Mater. 403, 48–61. https://doi.org/10.1016/j.jnucmat.2010.06.002.

Katoh, Y., Snead, L.L., Parish, C.M., Hinoki, T., 2013. Observation and possible mechanism of irradiation induced creep in ceramics. J. Nucl. Mater. 434, 141–151. https://doi.org/10.1016/j.jnucmat.2012.11.035.

Katoh, Y., Ozawa, K., Shih, C., Nozawa, T., Shinavski, R.J., Hasegawa, A., Snead, L.L., 2014. Continuous SiC fiber, CVI SiC matrix composites for nuclear applications: Properties and irradiation effects. J. Nucl. Mater. 448, 448–476. https://doi.org/10.1016/j.jnucmat.2013.06.040.

Kim, H.-G., Kim, I.-H., Jung, Y.-I., Park, D.-J., Yang, J.H., Koo, Y.-H., 2016. Development of Surface Modified Zr Cladding by Coating Technology for ATF. In: Top Fuel 2016, Boise, ID, pp. 1157–1163.

Koo, Y.-H., Yang, J.-H., Park, J.-Y., Kim, K.-S., Kim, H.-G., Kim, D.-J., Jung, Y.-I., Song, K.-W., 2014. KAERI's development of LWR accident-tolerant fuel. Nucl. Technol. 186, 295–304. https://doi.org/10.13182/NT13-89.

Snead, L., Shirvan, K., 2018. Wigner Energy in SiC and Implications to LWR Design, Nuclear Fuels & Structural Materials for Next Generation Nuclear Reactors Topical, American Nuclear Society, Philadelphia (June 2018).

Lee, Y., McKrell, T.J., Yue, C., Kazimi, M.S., 2013. Safety Assessment of SiC Cladding Oxidation under Loss-of-Coolant Accident Conditions in Light Water Reactors. Nucl. Technol. 183, 210–227. https://doi.org/10.13182/NT12-122.

Leistikow, S., Schanz, G., Berg, H.V., Aly, A.E., 1983. Comprehensive presentation of extended zircaloy-4 steam oxidation result (600-1600°C), OECD-NEA-CSNI/IAEA Spec. Meet. Water React. Fuel Saf. Fission Prod. Release off-Normal Accid. Cond. 16–20. https://inis.iaea.org/search/search.aspx?orig_q=RN:15059438 (accessed October 5, 2017).

Lemaignan, C., 2012. Zirconium alloys: properties and characteristics. In: Compr. Nucl. Mater.. Elsevier, pp. 217–232. https://doi.org/10.1016/B978-0-08-056033-5.00015-X.

Lillerud, K.P., 1980. On high temperature oxidation of chromium. J. Electrochem. Soc. 127, 2397. https://doi.org/10.1149/1.2129478.

Lipetzky, P., Dvorak, G.J., Stoloff, N.S., 1996. Tensile properties of a SiCf/SiC composite. Mater. Sci. Eng. A. 216, 11–19. https://doi.org/10.1016/0921-5093(96)10381-6.

Malik Wagih, K.S., Yifeng Che, 2017. Fuel Performance of Multi-Layered Zirconium Based Accident Tolerant Fuel Cladding. In: ICAPP, FUKUI & KYOTO, JAPAN.

Mieloszyk, A.J., 2015. Assessing thermo-mechanical performance of ThO2 and SiC clad light water reactor fuel rods with a modular simulation tool. https://dspace.mit.edu/handle/1721.1/103660?show=full (accessed January 19, 2018).

P.C. by Wilson, L., Mohr, C.L., Hesson, G.M., Wildung, N.J., Russcher, G.E., Webb, B.J., Freshley, M.D., 1993. NUREG/CR-3272 ;LOCA Simulation in NRU Program – Data Report for the Fourth Materials Experiment (MT-4). https://www.nrc.gov/docs/ML1019/ML101960140.pdf (accessed November 16, 2017).

Pint, B.A., Terrani, K.A., Brady, M.P., Cheng, T., Keiser, J.R., 2013. High temperature oxidation of fuel cladding candidate materials in steam-hydrogen environments. J. Nucl. Mater. 440, 420–427. https://doi.org/10.1016/j.jnucmat.2013.05.047.

Pint, B.A., Terrani, K.A., Yamamoto, Y., Snead, L.L., 2015. Material selection for accident tolerant fuel cladding. Metall. Mater. Trans. E. 2, 190–196. https://doi.org/10.1007/s40553-015-0056-7.

Price, R.J., 1977. Properties of Silicon Carbide for Nuclear Fuel Particle Coatings. Nucl. Technol. 35, 320–336. https://doi.org/10.13182/NT77-A31892.

Ševeček, M., Gurgen, A., Seshadri, A., Che, Y., Wagih, M., Phillips, B., Champagne, V., Shirvan, K., 2018. Development of Cr cold spray–coated fuel cladding with enhanced accident tolerance. Nucl. Eng. Technol. https://doi.org/10.1016/J.NET.2017.12.011.

Shah, H., Romero, J., Xu, P., Maier, B., Johnson, G., Walters, J., Dabney, T., Yeom, H., Sridharan, K., 2017. Development of surface coatings for enhanced accident tolerant fuel. Water React. Fuel Perform. Meet. 10.

Simmons G., 1965. Single crystal elastic constants and calculated aggregate properties.

Snead, L.L., Zinkle, S.J., White, D.P., 2005. Thermal conductivity degradation of ceramic materials due to low temperature, low dose neutron irradiation. J. Nucl. Mater. 340, 187–202. https://doi.org/10.1016/j.jnucmat.2004.11.009.

Snead, L.L., Nozawa, T., Katoh, Y., Byun, T.-S., Kondo, S., Petti, D.A., 2007. Handbook of SiC properties for fuel performance modeling. J. Nucl. Mater. 371, 329–377. https://doi.org/10.1016/j.jnucmat.2007.05.016.

Stephens, J., Klopp, W., 1972. High-Temperature Creep of Polycrystalline Chromium, Washington, DC. https://ntrs.nasa.gov/archive/nasa/casi.ntrs.nasa.gov/19720009851.pdf.

Stohl, A., Seibert, P., Wotawa, G., Arnold, D., Burkhart, J.F., Eckhardt, S., Tapia, C., Vargas, A., Yasunari, T.J., 2012. Xenon-133 and caesium-137 releases into the atmosphere from the Fukushima Dai-ichi nuclear power plant: determination of the source term, atmospheric dispersion, and deposition. Atmos. Chem. Phys. 12, 2313–2343. https://doi.org/10.5194/acp-12-2313-2012.

Stone, J.G., Schleicher, R., Deck, C.P., Jacobsen, G.M., Khalifa, H.E., Back, C.A., 2015. Stress analysis and probabilistic assessment of multi-layer SiC-based accident tolerant nuclear fuel cladding. J. Nucl. Mater. 466, 1–16. https://doi.org/10.1016/j.jnucmat.2015.08.001.

Sukjai, Y., 2014. Silicon carbide performance as cladding for advanced uranium and thorium fuels for light water reactors. https://dspace.mit.edu/handle/1721.1/87496#files-area (accessed January 8, 2018).

Terrani, K.A., Zinkle, S.J., Snead, L.L., 2014. Advanced oxidation-resistant iron-based alloys for LWR fuel cladding. J. Nucl. Mater. 448, 420–435. https://doi.org/10.1016/j.jnucmat.2013.06.041.

Weaver, C., 1968. Irradiation and the ductility of Chromium. Scr. Metall. 2, 463–466.

Williamson, R.L., Hales, J.D., Novascone, S.R., Tonks, M.R., Gaston, D.R., Permann, C.J., Andrs, D., Martineau, R.C., 2012. Multidimensional multiphysics simulation of nuclear fuel behavior. J. Nucl. Mater. 423, 149–163. https://doi.org/10.1016/j.jnucmat.2012.01.012.

Wilson, C.L., Hesson, G.M., Pilger, J.P., King, L.L., Panisko, F.E., 1993. Large-break LOCA, in-reactor fuel bundle Materials Test MT-6A.

Wu, X., Kozlowski, T., Hales, J.D., 2015. Neutronics and fuel performance evaluation of accident tolerant FeCrAl cladding under normal operation conditions. Ann. Nucl. Energy. 85, 763–775. https://doi.org/10.1016/j.anucene.2015.06.032.

Yamamoto, Y., Pint, B.A., Terrani, K.A., Field, K.G., Yang, Y., Snead, L.L., 2015. Development and property evaluation of nuclear grade wrought FeCrAl fuel cladding for light water reactors. J. Nucl. Mater. 467, 703–716. https://doi.org/10.1016/j.jnucmat.2015.10.019.

Zinkle, S.J., Terrani, K.A., Gehin, J.C., Ott, L.J., Snead, L.L., 2014. Accident tolerant fuels for LWRs: A perspective. J. Nucl. Mater. 448, 374–379. https://doi.org/10.1016/j.jnucmat.2013.12.005.